*Canadian Mineralogist*
Vol. 13, pp. 79-82 (1975)

# A NOTE ON THE POTENTIAL MINERALOGICAL APPLICATION OF NEUTRON RADIOGRAPHY

J. H. CROCKET, A. A. HARMS, AND L. A. HARTWIG
*Department of Geology and Department of Engineering Physics, McMaster University, Hamilton, Ontario, Canada L8S 4M1*

Developments in neutron imaging (Berger 1965; Herz 1969) and the increasing availability of intense neutron sources have prompted the wider use of neutrons in radiographic investigations in a variety of technical problem areas. Applications of this non-destructive radiographic method have been reported in such diverse areas as medicine (Brown & Parks 1969), archaeology (Robertson 1973), metallurgy (Reijonen & Forsten 1971), fluid flow (Moss & Kelly 1970) and rock fissures (Subramanian & Burkhart 1973) to name but some. Here we report on the potential use of neutron radiography in the diagnostic examination of mineralogical specimens.

The basic components of a neutron radiographic imaging system are illustrated in Figure 1. The essential features of neutron imaging can briefly be described as follows. A spatially-homogeneous beam of neutrons penetrates through a specimen of interest. This beam of neutrons is attenuated in its passage through the specimen according to the nuclear absorption properties of its constituent elements. Thus, the emerging beam of neutrons will possess a spatially dependent intensity pattern which, following a radiation conversion process in the converter foil, is subsequently recorded on the film emulsion in the form of a spatially varying optical density. The physical description of this conversion and imaging process has been reported elsewhere (Garside & Harms 1971; Harms & Norman 1972) and will not be described here. We mention that in the work reported upon here, we used standard industrial type $x$-ray film and a 25.4 $\mu$m thick gadolinium converter foil; the McMaster University Nuclear Reactor was used as the neutron source.

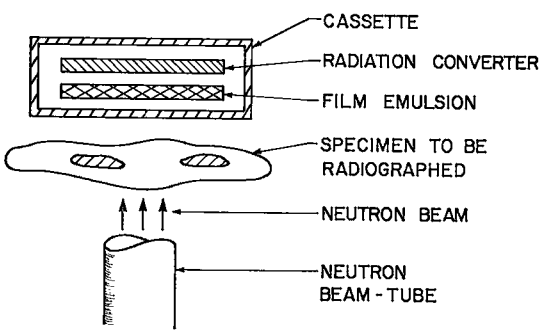


FIG. 1. Schematic representation of neutron radiographic system.

TABLE 1. LISTING OF RADIATION ATTENUATION PARAMETERS FOR X-RAYS AND NEUTRONS FOR SELECTED ELEMENTS

| Element | Atomic Number | Nominal Density | X-Ray Attenuation ($cm^2/g$ at 126 keV) | Neutron Absorption ($10^{-24} cm^2$ at 0.025ev) |
|---|---|---|---|---|
| B | 5 | 2.3 $g/cm^3$ | 0.14 | 759 |
| Mn | 25 | 7.4 | 0.25 | 13 |
| Ag | 47 | 10.5 | 1.05 | 64 |
| Cd | 48 | 8.6 | 1.09 | 2450 |
| Sn | 50 | 7.3 | 1.11 | 0.63 |
| Gd | 64 | 7.9 | 2.08 | 46,000 |
| Au | 79 | 19.3 | 3.21 | 98.8 |
| U | 92 | 19.1 | 3.90 | 7.6 |

The dimensional unit $10^{-24} cm^2$ is defined as a barn, abbreviated "b"

The method of obtaining neutron radiographic images is very similar to that employed in $x$-ray and $\gamma$-ray radiography; however, the resultant images and their interpretation differ in a most fundamental way. While the attenuation of $x$-rays and $\gamma$-rays is to a large extent a material–density phenomenon, the attenuation of neutrons is determined primarily by the absorption cross-section of the elements. Since cross-section characteristics have been found to bear no relationship to material density, conditions thus exist to provide complementary — if not distinct — radiographic information. In Table 1 we list several elements and their corresponding radiation attenuation parameters for both $x$-rays and neutrons. Here we note the considerable variation in the neutron absorption cross-section for the various elements.

Neutron absorption cross-sections have been measured for most elements. An equivalent absorption cross-section can be defined for any compound by a suitable summation. For example, the absorption cross-section for the compound identified by the molecular formula $X_mY_n$ can — under conditions which generally apply in neutron radiography — be represented by

$$\sigma_{X_mY_n} = m\sigma_X + n\sigma_Y \ , \ldots\ldots\ldots \quad (1)$$

where the absorption cross-sections for elements $X$ and $Y$, given by $\sigma_X$ and $\sigma_Y$ respectively, may

be extracted from any one of several tabulations. Thus, the absorption cross-section for pyrite ($FeS_2$) is clearly

$$\sigma_{FeS_2} = 1\sigma_{Fe} + 2\sigma_{S_2}$$
$$= 1 \times 2.6 \text{ barns} + 2 \times 0.5 \text{ barns} \quad (2)$$
$$= 3.6 \text{ barns}$$

Here we have used the usual unit for cross-section named a "barn" which is defined as $10^{-24}cm^2$. This unit for the absorption cross-section will be used in our subsequent discussion on the absorption characteristics of neutrons in minerals.

In Figure 2 we show the results of a radiographic examination of a 1.5 cm thick section of a **drill core sample from the Silverfields mine,** Cobalt, Ontario. The principal mineral constituents are cobaltite (Co,Ni) AsS, nickeline NiAs,

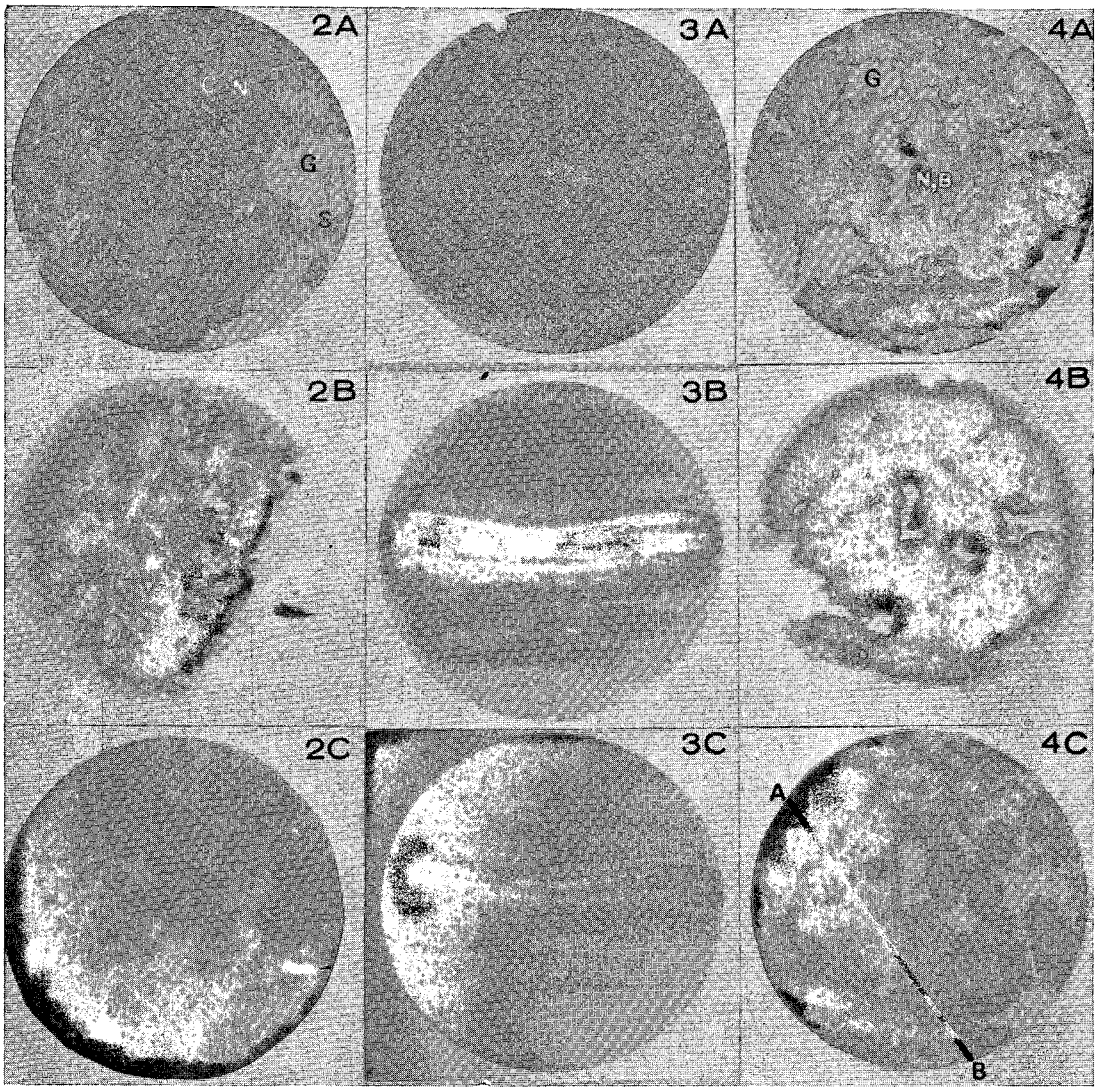


FIG. 2. Sulpharsenide sample: A(top) polished surface in plain light showing carbonate gangue (G), silver veinlet (S), and cobaltite and nickeline (C,N); B *x*-ray image; C neutron image.

FIG. 3. Base metal sulphide sample: A(top) polished surface in plain light showing sphalerite-rich band (SP) and pyrite-rich domain (P); (B) *x*-ray image; (C) neutron image.

FIG. 4. Arsenide-antimonide sample: A(top) polished surface in plain light showing nickeline and breithauptite (N,B), and carbonate gangue (G); (B) *x*-ray image; (C)- neutron image. Scan path A-B shown in Figure 5.

native silver, native bismuth and carbonate, mainly calcite. The distribution of these phases may be seen, in part, from the polished section photograph (Fig. 2A). The carbonate gangue occurs as a massive area on the edge of the slide —where it contains native metal veinlets — and as irregular patches within the arsenides where it is devoid of silver or bismuth. Cobaltite comprises the bulk of the arsenide portion of the section. It contains about 10% nickeline — not visible in the photograph — distributed uniformly throughout the cobaltite.

The contrast in neutron absorption for the carbonate gangue and the arsenides is large in that $\sigma_{\text{cobaltite}}/\sigma_{\text{calcite}} \simeq 42/0.43 = 98$. Nickel substitution for cobalt will decrease $\sigma_{\text{cobaltite}}$ but even for the most nickel-rich cobaltites noted by Petruk *et al.* (1971), the contrast in neutron absorption between the arsenides and gangue will be at least 50:1.

Both the *x*-ray and neutron radiographs clearly differentiate the arsenide and carbonate gangue domains with the neutron image providing good detail of the gangue-arsenide relationships in the arsenide domain. Both images show the silver veinlet in the gangue. Thus some of the information obtained from both techniques is of a complementary nature. However, certain aspects of the neutron imagery provide diagnostic information not apparent from the *x*-ray radiograph. Firstly, in the neutron image the silver veinlet produces a darker tone of grey than the arsenide domain. This indicates a difference in elemental composition with the former representing the better neutron absorber. The effect results from the 64 barn absorption cross-section of silver which is significantly higher than the 21 to 42 barn cross-section of cobaltite. There is no suggestion from the *x*-ray image that the silver and arsenide domains differ in composition. Secondly, more detail on the silver veining in carbonate gangue is obtained in the neutron image where veinlets as small as 0.03 mm in width are easily distinguished.

In Figure 3 we show results obtained from a base metal ore sample from the Heath Steele deposit, Bathurst district, New Brunswick. The specimen consists principally of pyrite ($FeS_2$), sphalerite (Zn,Fe)S, galena (PbS) and silicate gangue consisting mainly of quartz. A distinctive banding results from varying proportions of sphalerite and galena in a pyrite matrix; one distinctively sphalerite-rich band is obvious in the middle of the section (Fig. 3A). The sphalerite bands, particularly the massive one, are well-differentiated on the *x*-ray image and are distinct on the neutron image. The detail on the massive band which is not apparent in the optical photograph is due in part to a divergence of about 10° between the *x*-ray and neutron beams and the inclination of the sphalerite-rich bands. The *x*-ray image reflects, as expected, the superior attenuation of zinc relative to iron. The neutron image, which is superficially similar, indicates that sphalerite is a better neutron absorber than pyrite. This result is not obvious and would not be predicted from the neutron absorption cross-sections of pyrite and sphalerite applicable to pure phases. For pyrite taken as $FeS_2$ and sphalerite as $(Zn_{0.9}Fe_{0.1})S$, cross-sections of 3.6 and 1.8 barns respectively, apply. Thus, sphalerite domains should be poorer absorbers than pyrite domains, the reverse of what is actually found.

We suggest that the explanation of this apparent reversal of neutron absorption results in part from minor element impurities which have a significant effect on the neutron absorption properties of the minerals. The compositions of Heath Steele sphalerites and pyrites recorded by Sutherland & Halls (1969) and Sutherland (1967) show that cadmium is strongly concentrated in the sphalerite. As $\sigma_{Cd} = 2450$ barns, a significant absorption contribution from this element will occur. For average sphalerite and pyrite compositions calculated from their analyses, cross-sections of 3.3 and 3.8 barns respectively are computed. Trace Cd, 0.026 mole %, accounts for 43% of the total neutron absorption in sphalerite whereas the only significant absorbers in pyrite, other than the major elements, are Cd and Co which account for 5%. Thus, Heath Steele pyrite is only a slightly better neutron absorber than sphalerite. This property, coupled with a significantly higher abundance of silicate inclusions in the pyrite relative to the sphalerite domains, is considered to account for the major features of the neutron image. The neutron image then strongly infers compositional properties of these domains which would not be deduced from the *x*-ray image alone.

As a final example we illustrate the possibility of quantitative analysis of radiographic images from a microdensitometer scan. The sample, (Fig. 4) is a mixed arsenide-antimonide of cobalt and nickel from the Cobalt area, Ontario. The optical density variation along the traverse A-B for both images is shown in Figure 5.

The sample consists mainly of nickeline (NiAs), breithauptite (NiSb) and minor cobaltite ( (Co, Fe)AsS) in a carbonate gangue. The nickeline and breithaupite form crudely spherical, coalescing aggregates. The main contrast in neutron absorption is between the calcite gangue ($\sigma_{\text{calcite}} = 0.4$ barns) and the arsenide-antimonide domains ($\sigma_{\text{nickeline}} = 8.8$ barns, $\sigma_{\text{breithauptite}} = 9.7$ barns whereas $\sigma_{\text{cobaltite}}$ varies from 21 barns

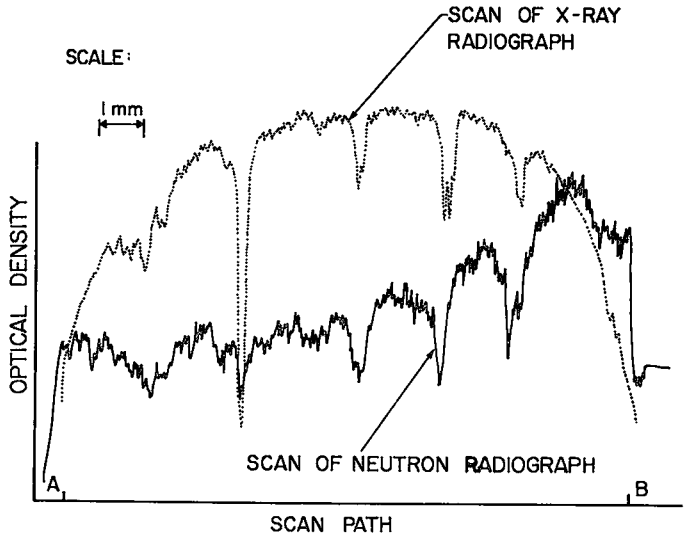


FIG. 5. Microdensitometer scans of *x*-ray image 4B and neutron image 4C. Scan path, shown on the neutron image only, is A-B.

to 42 barns depending on composition). The *x*-ray image shows little detail in the arsenide-antimonide domain whereas the neutron radiography very clearly reveals the rounded, globular nature of these aggregates. Little internal detail, however, is obtained because the nickeline-breithauptite neutron absorption cross-sections are similar, and cobaltite — although a much better neutron absorber — is a minor phase widely dispersed as single crystals throughout the mass.

The microdensitometer profiles for both the *x*-ray and neutron images clearly delineate the carbonate and antimonide-arsenide domains. The neutron scan gives better resolvability of structure near the sample margins than the *x*-ray scan.

The unique penetration characteristics of neutrons therefore serve a definite complementary role in the radiographic examination of mineralogical samples. It is clear that the utility of such a diagnostic method will be most effective where significant differences in isotopic cross-section, not necessarily correlated with material density, characterize the material of interest.

## ACKNOWLEDGEMENTS

This study was supported by a grant from the Science and Engineering Research Board, McMaster University.

## REFERENCES

BERGER, H. (1965): *Neutron Radiography*. Elsevier, New York.

BROWN, M. & PARKS, P. B. (1969): Neutron radiography in biological media. *Amer. J. Roentgenology* **106**, 472-485.

GARSIDE, B. K. & HARMS, A. A. (1971): The detection process in neutron radiography. *J. Appl. Physics* 42, 5161-5167.

HARMS, A. A. & NORMAN, G. R. (1972): The role of internal conversion electrons in gadolium-exposure neutron imaging. *J. Appl. Physics* **43**, 3209-3212.

HERTZ, R. H. (1969): *The Photographic Action of Ionizing Radiations*. Wiley-Interscience, New York.

MOSS, R. A. & KELLY, A. J. (1970): Neutron radiography study of limiting planar heat pipe performance. *Internat. J. Heat Mass Transfer* **13**, 491-502.

PETRUK, W., HARRIS, D. C. & STEWART, J. M. (1971): Characteristics of the arsenide, sulpharsenides, and antimonides. In *The Silver-Arsenide Deposits of the Cobalt-Gowganda Region, Ontario. Can. Mineral.* **11**, 150-186.

REIJONEN, H. & FORSTEN, J. (1971): Neutron radiography of unidirectionally solidifying Sn-Cd alloys. *Metallurgical Trans.* **2**, 1921-1924.

ROBERTSON, T. J. M. (1973): Neutron applications to archaeology. *Atomic Energy Res. Establ.*, Harwell, Berks, U.K.

SUBRAMANIAN, R. V. & BURKHARDT, D. (1973): Determination by neutron radiography of the location of polymeric resins injected in rock fissures. *Nucl. Technology* **17**, 184-188.

SUTHERLAND, J. K. (1967): The chemistry of some New Brunswick pyrites. *Can. Mineral.* **9**, 71-84.

——— & HALLS, C. (1969): Composition of some New Brunswick sphalerites. *Research Note* **21**, *New Brunswick Res. Productivity Council.*

*Manuscript received May 1974.*